Electronic Supplementary Information

Strong metal-support interactions for high sintering resistance of Ru-based catalysts toward HER and ORR

Xuzhuo Sun,[a] Baofan Wu,[a] Bo Li,[a] Jiashou Zhao,[a] Shanshan Li,[a] Mai Zheng,[b] Jing Chen *[a] and Haibo Zhang *[b]

[a] College of Chemistry and Chemical Engineering, Henan University of Technology, Zhengzhou 450001, PR China. E-mail: chenjing0504@haut.edu.cn

[b] College of Chemistry and Molecular Sciences and National Demonstration Center for Experimental Chemistry, Wuhan University, Wuhan 430072, PR China. E-mail: haibozhang1980@gmail.com

Table of Contents

1. Experimental

1.1 Materials and Chemicals

Cs_2[*closo*-$B_{12}H_{12}$], Tris(2,2'-bipyridine)ruthenium(II) chloride hexahydrate ($Ru(bpy)_3Cl_2$), was purchased from Aladdin Chemical Reagent Co., Ltd., and used as received. 5 wt% Nafion aqueous solution was purchased from Sigma-Aldrich. 20 wt% Pt/C purchased from Alfa Aesar. All chemicals were of analytical grade and used without further purification.

1.2 Synthesis of Ru-BOPs

74.863 mg (0.1 mmol) $Ru(bpy)_3Cl_2$ was dissolved in 20 mL water, and 40.7 mg (0.1 mmol) Cs_2[*closo*-$B_{12}H_{12}$] was dissolved in 20 mL H_2O. When these two solutions mixed together, a large amount of orange-red solid was immediately produced. After stirring for 2 h, the solids were collected by centrifugation and washed alternately with ethanol and water three times, then dried under vacuum at 60 °C for 8 h. The product was named Ru-BOPs.

374.3 mg (0.5 mmol) $Ru(bpy)_3Cl_2$ was dissolved in 100 mL water, and 40.7 mg (0.1 mmol) Cs_2[*closo*-$B_{12}H_{12}$] was dissolved in 20 mL H_2O After mixing together and stirring for 2h, the solids were collected by removing water through rotational evaporation, then dried under vacuum at 60 °C for 8 h. The product was named Ru-BOPs-0.2.

Ru-BOPs-5 was prepared in the same way by changing the mole ratio of $Ru(bpy)_3Cl_2$ and Cs_2[*closo*-$B_{12}H_{12}$] to 1:5.

1.3 Synthesis of RuBCN

The procedure for preparing RuBCN by pyrolysis of Ru-BOPs is as follows. In N_2 atmosphere, Ru-BOPs was calcinated by raising temperature to 800 °C with a heating rate of 5 °C/min and kept for 2 h, and then RuBCN was obtained after naturally cooling to room temperature.

Ru-BOPs samples were pyrolyzed with similar procedure by changing 800 °C to 700℃ and 900℃, and the obtained samples were named RuBCN-700 and RuBCN-900.

Ru-BOPs-0.2 and Ru-BOPs-5 were pyrolyzed at 800℃ with same procedure, and the obtained samples were named RuBCN-0.2 and RuBCN-5.

1.4 Synthesis of RuCN

RuCN was prepared by direct pyrolysis of $Ru(bpy)_3Cl_2$ with same procedure of RuBCN.

The samples obtained by changing the calcination temperature to 700℃ and 900℃ were named RuCN-700 and RuCN-900.

1.5 Characterization Method

The Fourier transform infrared (FT-IR) spectra of the material were recorded on an infrared spectrometer (Thermo iS10), with a spectral range from 400 cm^{-1} to 4000 cm^{-1}. The Bruker D8 Advance powder X-ray diffractometer (Cu Kα radiation source) was used for recording the powder X-ray diffraction (XRD) patterns, 2θ range from 5° to 80°. Raman spectra data were recorded at ambient temperature with a Renishaw Microscope System RM2000 Raman spectrometer. Raman spectra were collected with a Thermo Electron Corporation DXR Microscope. X-ray photoelectron spectroscopy (XPS) were recorded on a PHI5000VersaProbell using Al Kα X-ray source to analyse the elements binding states. The morphology of the samples was characterized by transmission electron microscope (TEM, FEI Tecnai G220), scanning electron microscope (SEM, QUANTA FEG 250), and energy dispersive X-ray spectrum (EDS) elemental mapping. The content of Ru was obtained by inductively coupled plasma-optical emission spectrometer (ICP-OES) (Aglient 5110).

1.6 Electrochemical Hydrogen Evolution Reaction (HER) Studies

All electrochemical measurements were performed using a CHI Electrochemical Station (Model 660E) in a conventional three-electrode cell at room temperature (25 °C). Graphite rod was used as counter electrode. Ag/AgCl was used as the reference electrode. The working electrode was prepared as follows: the catalyst powder (5 mg) and carbon black (10 mg) were dispersed in a mixture solution of 5 wt% Nafion solution (200 μL) and 1500 μL isopropyl alcohol, followed by ultrasonication for 30 min to form

homogeneous ink. Then 42.5μL of the mixture was subsequently dropped on a 0.5×0.5 cm^2 carbon paper with mass loading of 0.5 mg cm^{-2} and dried at room temperature. Moreover, 1.0 M KOH and 0.5 M H_2SO_4 were used as the alkali and acid, respectively. All polarization curves were corrected by iR. All the potentials mentioned in this work were calibrated with respect to reversible hydrogen electrode (RHE) based on the following equation:

$$E(\text{vs.}RHE) = E(\text{vs.}Ag/AgCl) + 0.059\text{p}H + 0.197 - 0.9iR$$

All the linear sweep voltammetry (LSV) of the catalysts was measured in N_2-saturated water solution. The HER polarization data were obtained by LSV at a scan rate of 5 mV s^{-1}. Accelerated durability test was performed by cyclic voltammetry (CV) experiments with a scan rate of 100 mV s^{-1}. The Tafel slopes were calculated according to the Tafel equation η= b log (j/j_0) based on the LSV curves, where η is the overpotential, b is the Tafel slope, j is the current density, and j_0 is the exchange current density. The mass activity value (mA μg^{-1}) was calculated from the electrocatalyst loading mass m (0.5 mg cm^{-2}) and the measured current density j (mA cm^{-2}) at different potentials:

$$\text{Mass activity} = \frac{j}{m \times 10^{3} \times wt\%\,(metal)}$$

wt% (metal) is the value of weight percentage of noble metal based on the ICP-OES result.

Electrochemical impedance spectroscopy (EIS) tests were collected ranging from 0.01 Hz to 100 kHz with an amplitude of 5 mV at an initial voltage of 10 mA cm^{-2}. The double-layer capacitance (C_{dl}) was measured to obtain electrochemically active surface area (ECSA) by using cyclic voltammetry scans measurement at non-Faraday reaction range from 0.19 V to 0.31 V (vs. RHE) with different scan rates (ν, 10–50 mV s^{-1}). The value of C_{dl}, was obtained by the equation $C_{dl} = \Delta j/\nu$, where Δj were halves of the difference between the anodic and cathodic current densities (j_a and j_c) at 0.25 V (vs. RHE), that is $\Delta j = (j_a - j_c)/2$. The long-term stability tests were carried out by

chronoamperometric measurements (i-t curves) with fixing potentials at 10 mA cm^{-2}.

1.7 Electrochemical Oxygen Reduction Reaction (ORR) Studies

ORR studies were performed in a typical three-electrode configuration using CHI Electrochemical Station (Model 760E) with a rotating disk electrode (RDE) and rotating ring disk method (RRDE) of the Pine instrument. The Ag/AgCl with saturated KCl solution, graphite rod, and the rotating disk electrode (RDE, d = 5.0 mm) or rotating ring-disk electrode (RRDE, d = 5.61 mm) were used as reference electrode, counter electrode and working electrode, respectively. The preparation of electrode ink is the same as HER. The loading mass of electrocatalysts on RDE or RRDE working electrode was 0.5 mg cm^{-2}. Before recording the linear scan voltammogram (LSV) curves of ORR, several cycles of cyclic voltammetry (CV) at the scan rate of 50 mV s^{-1} were carried out to activate the catalysts and reach a relatively steady state. RDE measurements were carried out at different speeds from 400 to 2025 rpm in N_2 and O_2 saturated 0.1 M KOH aqueous solution. The stability was adjudged by linear sweep voltammetry (LSV) up to 5000 cycles with a scan rate of 100 mV s^{-1} at a rotation speed of 1600 rpm. Chronoamperometry was used to investigate the durability and the methanol tolerance of catalysts with the fixed potential 0.7 V (vs. RHE) at 1600 rpm.

The peroxide yield (H_2O^-) and the number of transferred electrons (n) were calculated by the below equations.

$$n = 4\frac{I_d}{I_r / N + I_d}$$

$$H_2O^-(\%) = 100\frac{2I_r / N}{I_d + I_r / N}$$

where I_d and I_r are the disk and ring currents, respectively, and N = 0.37 is the collection efficiency of the Pt ring.

The ORR reaction kinetics was calculated by Koutecký-Levich equation:

$$\frac{1}{j}=\frac{1}{j_l}+\frac{1}{j_k}=\frac{1}{B\omega^{1/2}}+\frac{1}{j_k}$$

$$B=0.2nFC_{O2}D^{2/3}\nu^{-1/6}$$

Where j, j_l, and j_k is the measured current density, diffusion-limiting current density, and kinetic current density, respectively. The ω represent the electrode's angular velocity. n is the number of electrons, F is the Faraday constant (F = 96,485 C mol^{-1}), C_{O2} is the saturated O_2 concentration (1.21×10^{-6} mol cm^{-3}), D is the diffusion coefficient of O_2 in 0.1 M KOH (1.9×10^{-5} cm^2 s^{-1}) and ν is the kinetic viscosity (0.01 cm^2 s^{-1}).

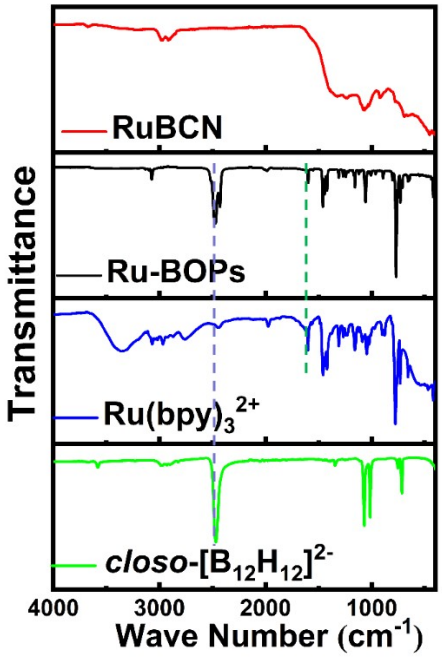

Fig S1. FT-IR spectrum of *closo*-$[B_{12}H_{12}]^{2-}$, $Ru(bpy)_3^{2+}$, Ru-BOPs and RuBCN.

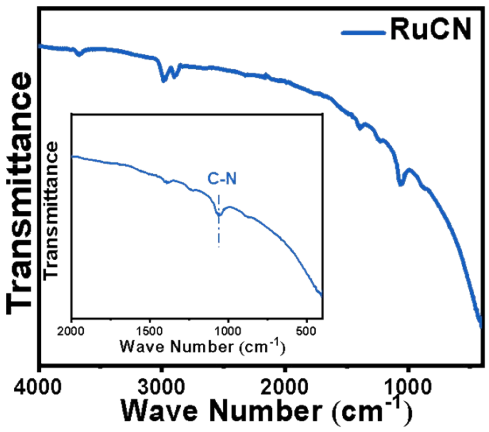

Fig S2. FT-IR spectrum of RuCN.

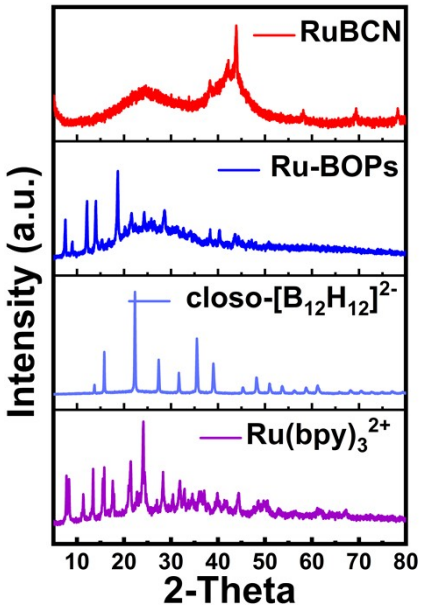

Fig S3. XRD images of $Ru(bpy)_3^{2+}$, *closo*-$[B_{12}H_{12}]^{2-}$, Ru-BOPs and RuBCN.

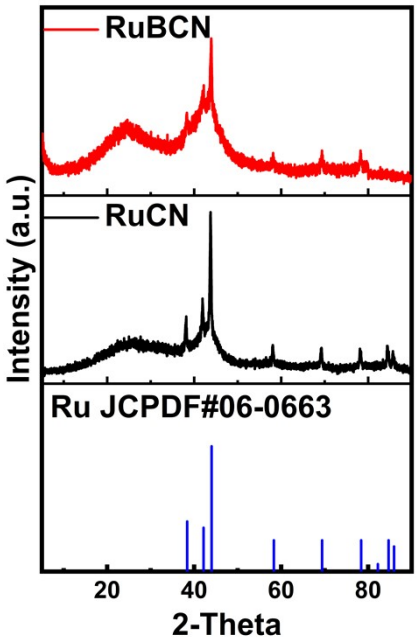

Fig S4. XRD images of RuBCN and RuCN.

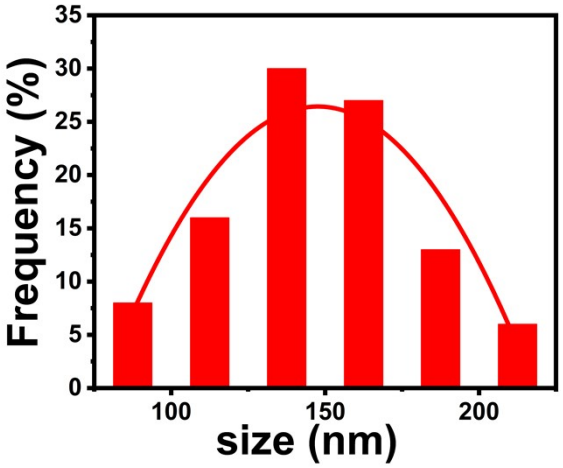

Fig S5. The particles size distribution of RuBCN.

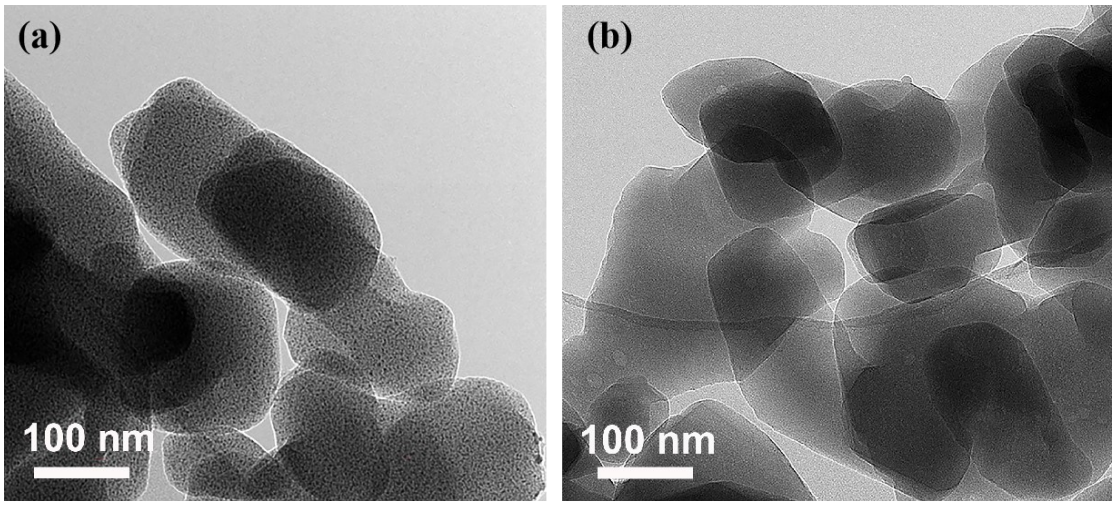

Fig S6. The TEM images of RuBCN and Ru-BOPs.

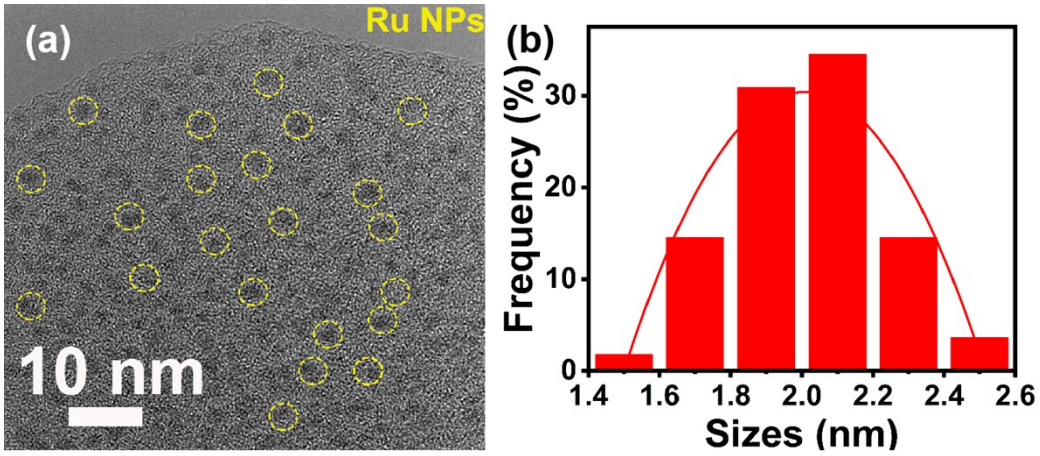

Fig S7. The particles size of RuNPs on RuBCN. (a) TEM image, (b) size distribution.

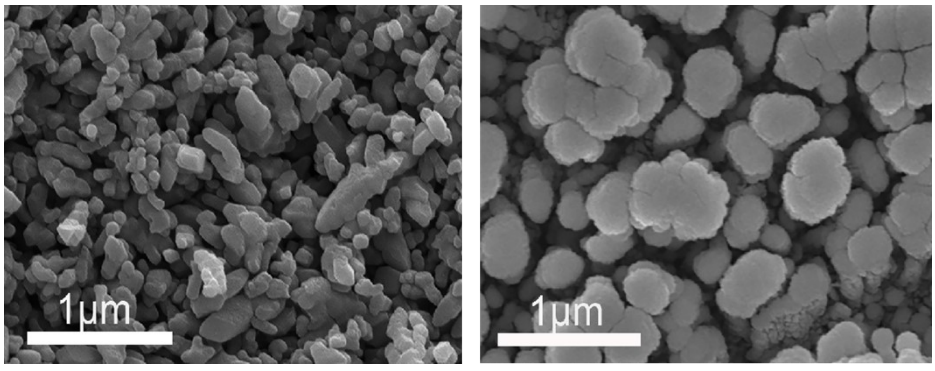

Fig S8. The SEM images of RuBCN and RuCN.

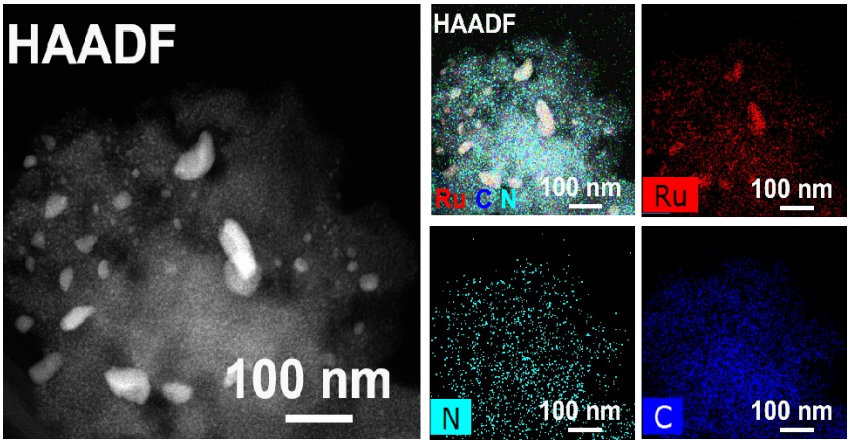

Fig S9. Element (B, C, N, Ru) mapping images of RuCN.

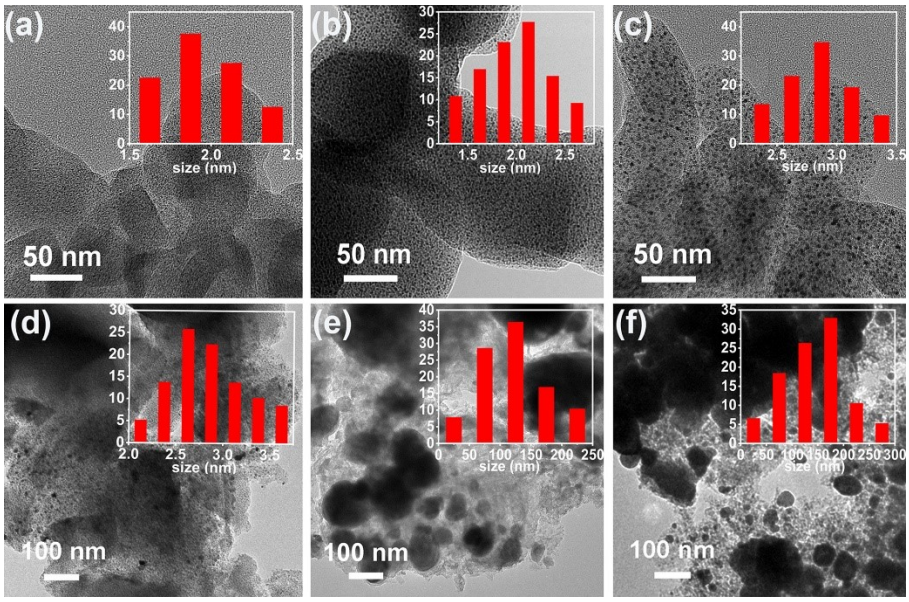

Fig S10. The TEM images of (a-c) RuBCN-700, RuBCN, and RuBCN-900, (d-f) RuCN-700, RuCN and RuCN-900.

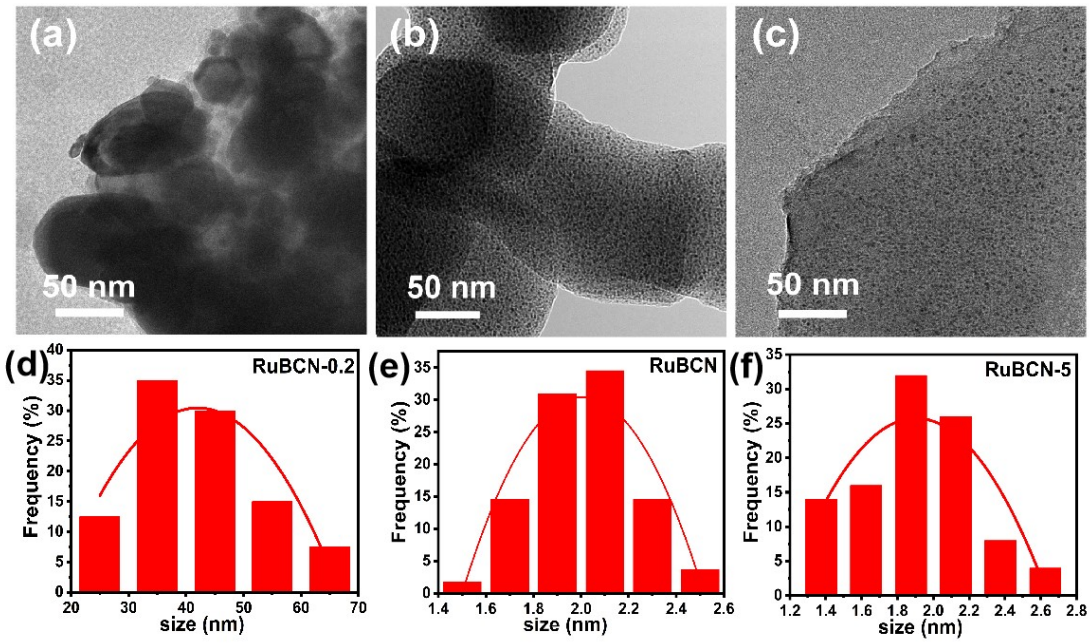

Fig S11. The TEM images of (a) RuBCN-0.2, (b) RuBCN, (c)RuBCN-5.

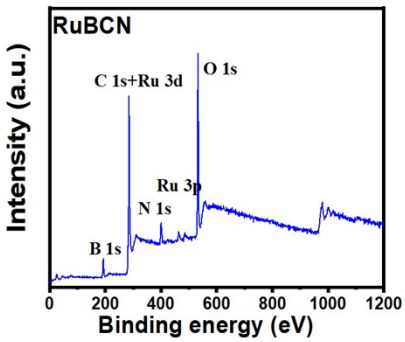

	B1s	C1s	N1s
RuBCN Atomic %	11.0	79.5	9.5

Fig S12. XPS survey spectrum data of RuBCN and the elemental content ratio of B, N and C.

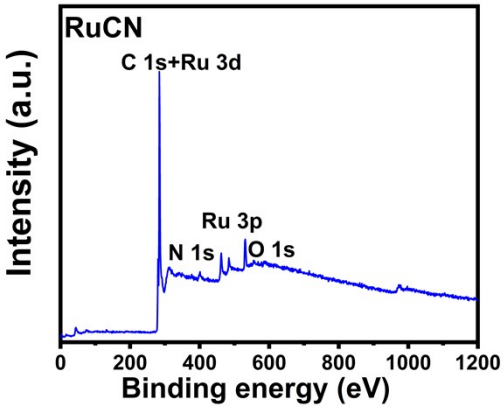

Fig S13. XPS survey spectrum data of RuCN.

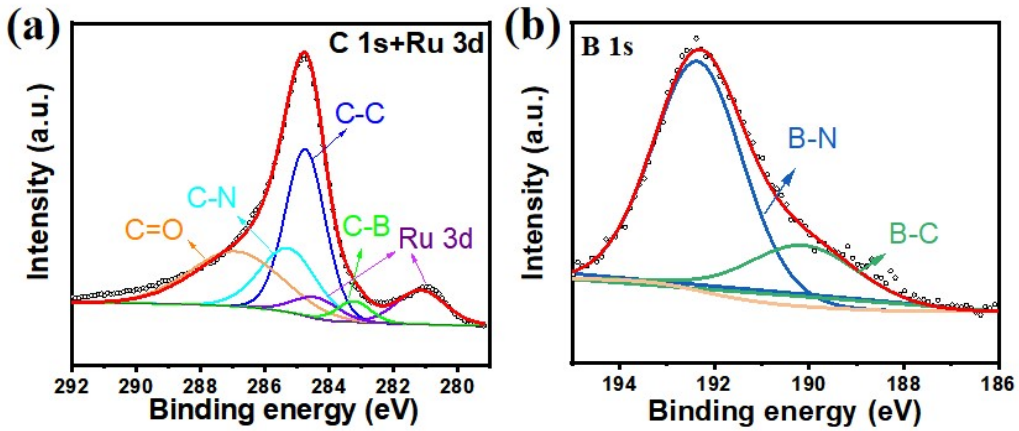

Fig S14. High-resolution XPS spectra of (a) C 1s and Ru 3d of RuBCN; (b) B 1s of RuBCN.

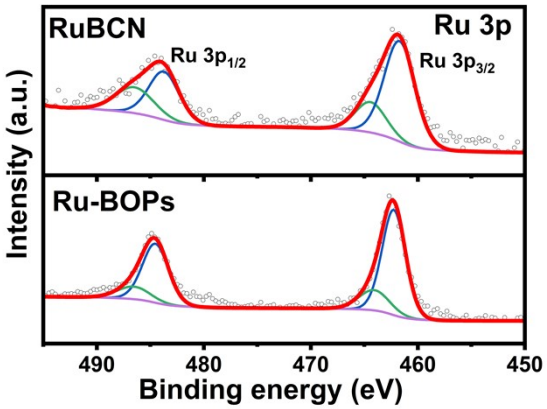

Fig S15. High-resolution XPS spectra of Ru 3p of RuBCN and Ru-BOFs.

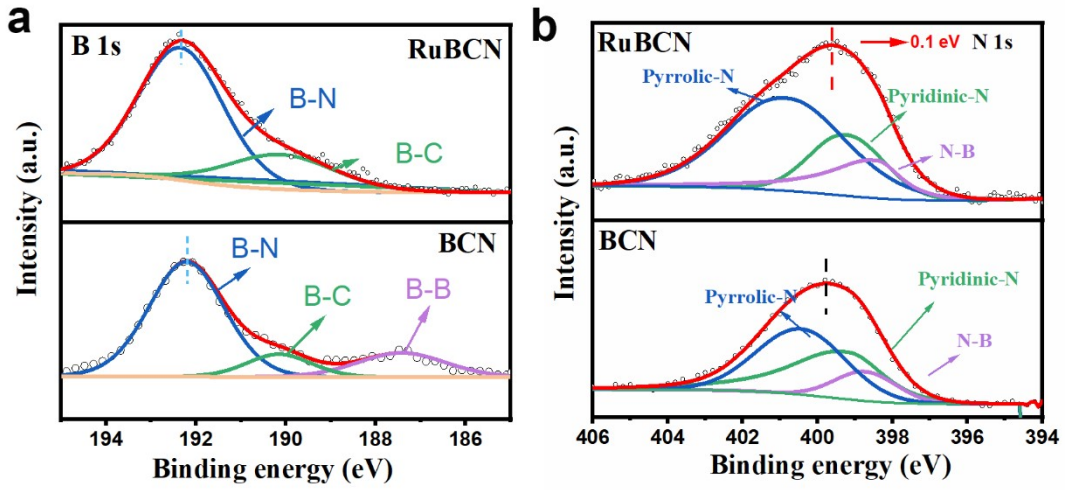

Fig S16. The XPS data of RuBCN and BCN. (a) B1s, (b) N1s.

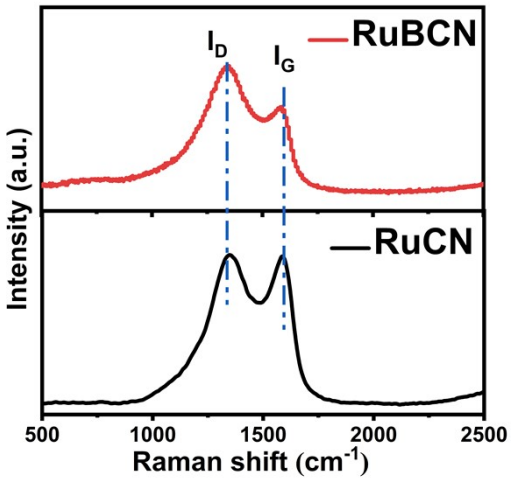

Fig S17. Raman spectra of RuBCN and RuCN.

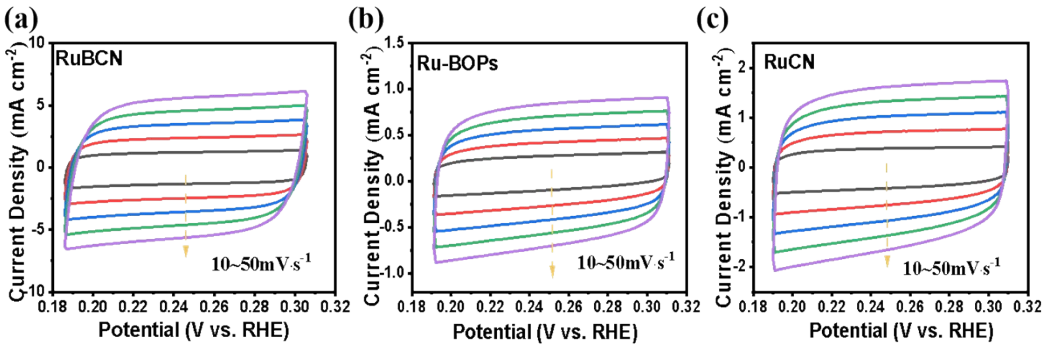

Fig S18. Cyclic voltammetry with different scan rates (10-50 mV s^{-1}) in 1.0 M KOH solution for HER (a) RuBCN, (b) Ru-BOPs, (c) RuCN.

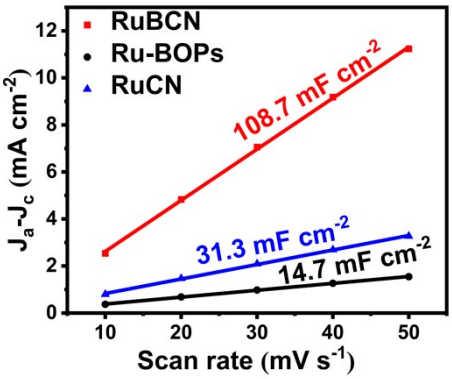

Fig S19. C_{dl} of RuBCN, Ru-BOPs and RuCN in alkaline solution.

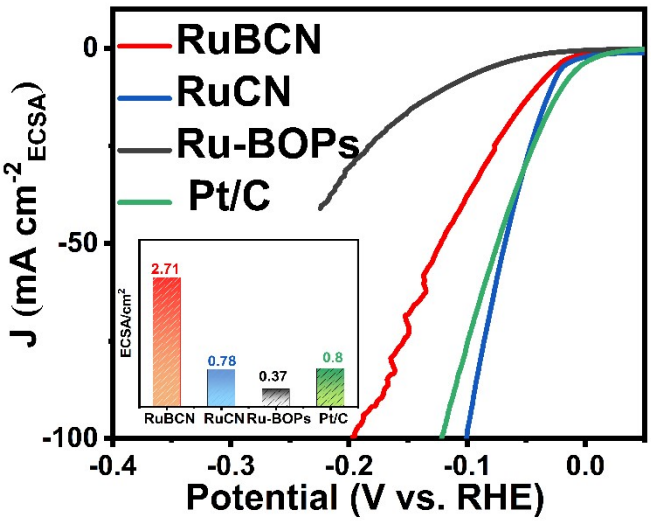

Fig S20. The ECSA-normalized LSV curves of catalysts.

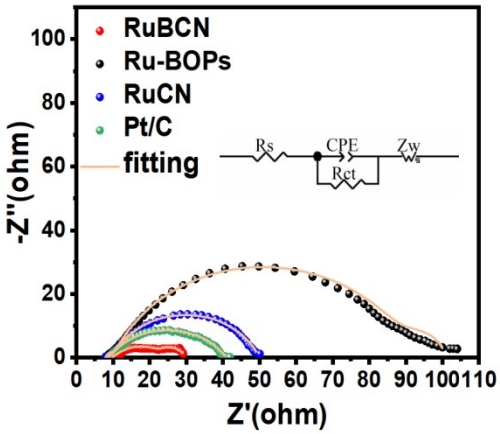

Sample	R_s (Ω)	R_{ct} (Ω)
RuBCN	9.2	21.9
Ru-BOPs	9.0	84.9
RuCN	8.8	42.5
Pt/C	8.8	32.3

Fig S21. The comparison of EIS for HER activity in alkaline solution.

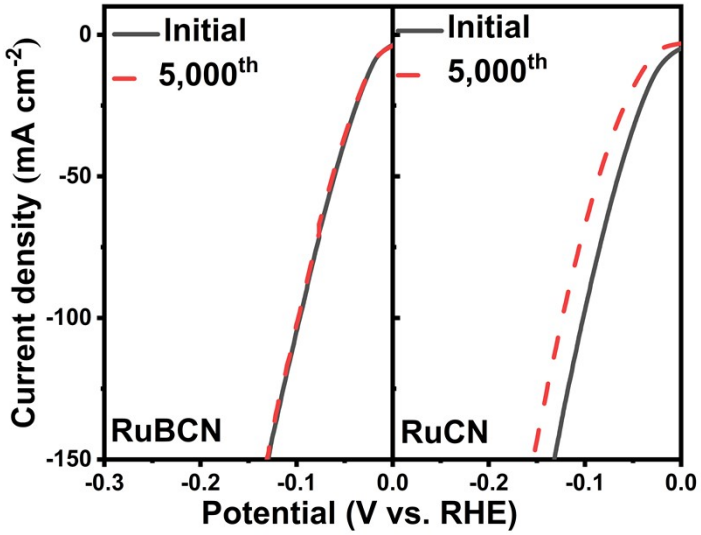

Fig S22. The polarization curves of RuBCN and RuCN before and after 5,000 cycles in 1.0 M KOH.

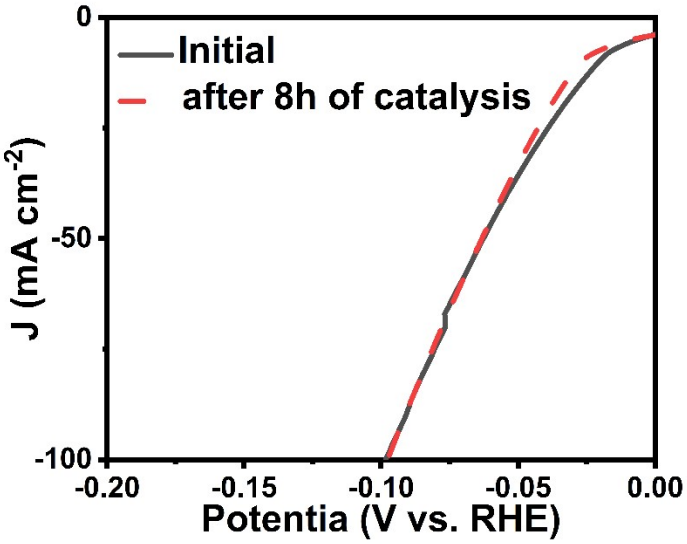

Fig S23. The polarization curves of RuBCN before and after 8h of catalysis in 1.0 M KOH.

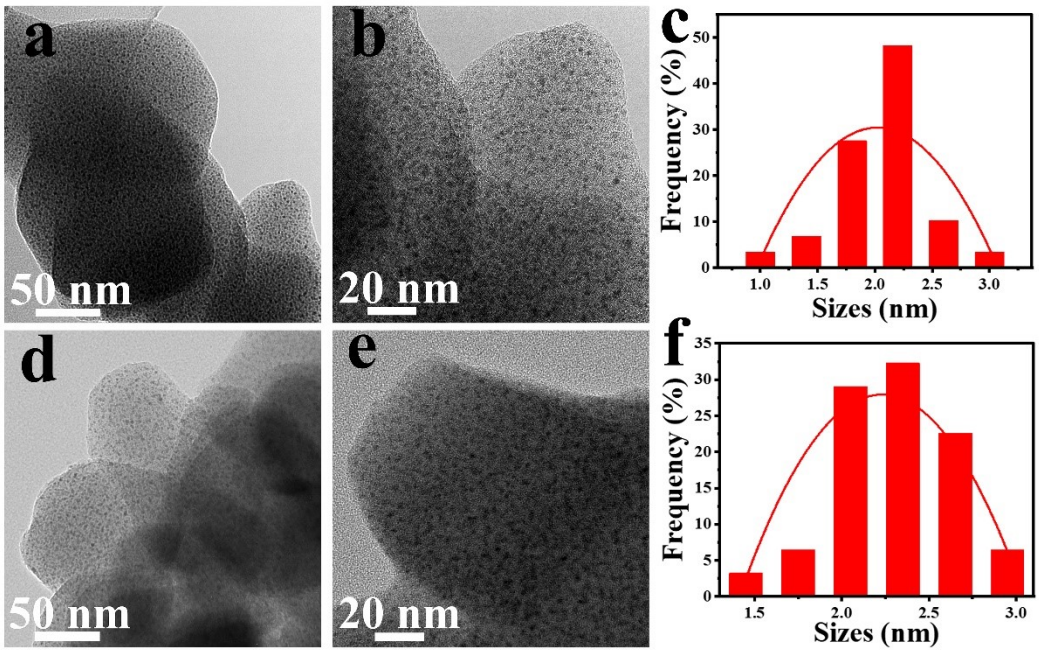

Fig S24. the TEM images of RuBCN before and after long-term electrocatalysis

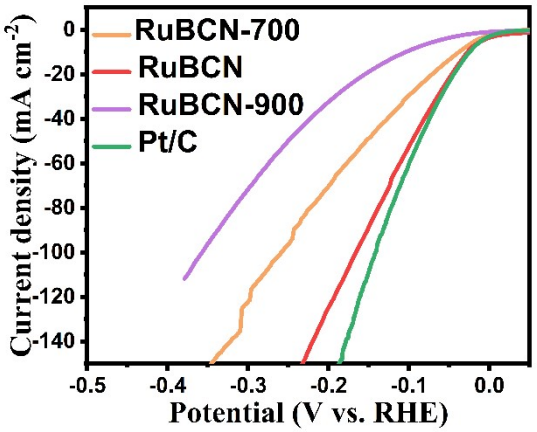

Fig S25. The polarization curves of RuBCN-700, RuBCN, RuBCN-900 and Pt/C in 1 M KOH.

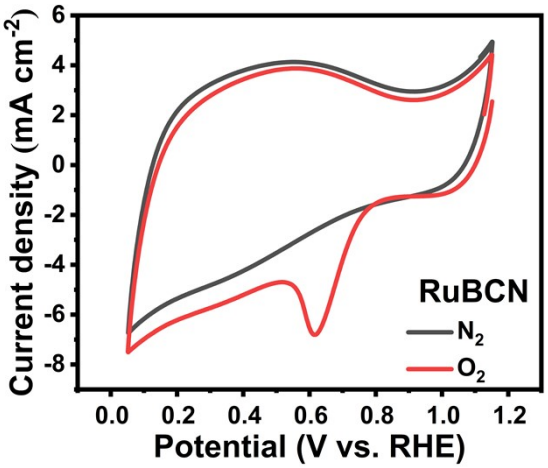

Fig S26. CV curves of RuBCN in N_2- and O_2-saturated 0.1 M KOH electrolyte at a scan rate of 50 mV/s.

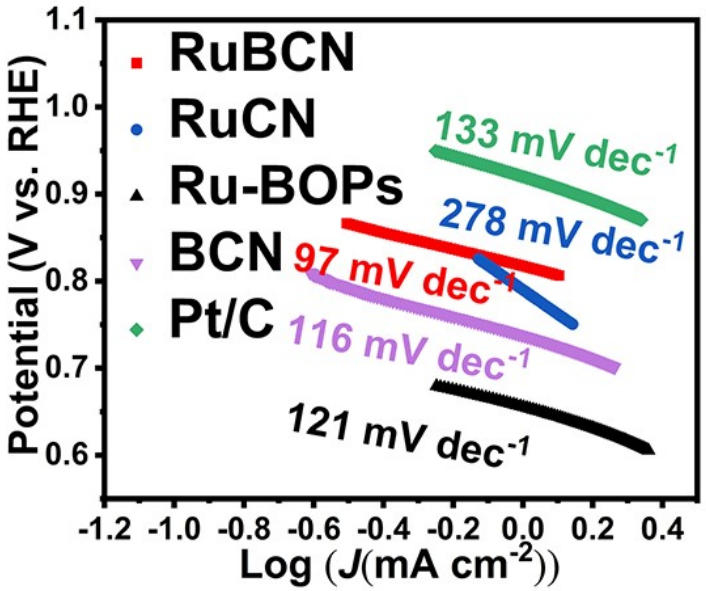

Fig S27. Tafel slopes corresponding to ORR polarization curves.

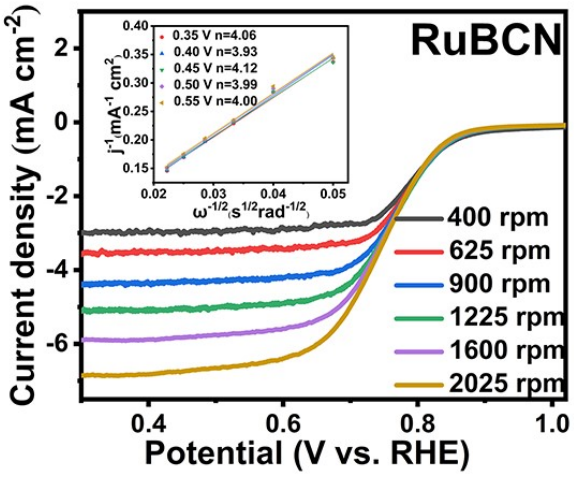

Fig S28. LSV curves of RuBCN recorded at various rotation speeds with insetting corresponding K–L plots at different potentials.

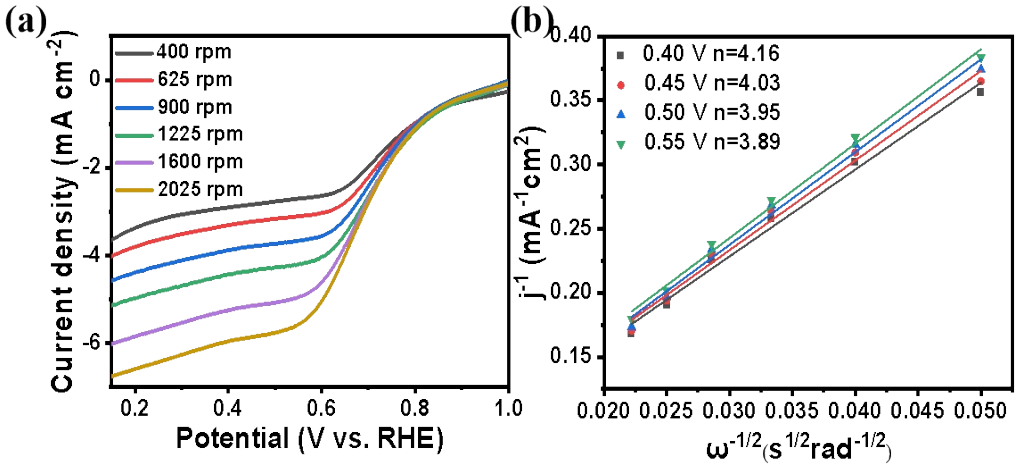

Fig S29. (a) LSV curves at different rotation speeds of RuCN. (b) K−L plot of the RuCN.

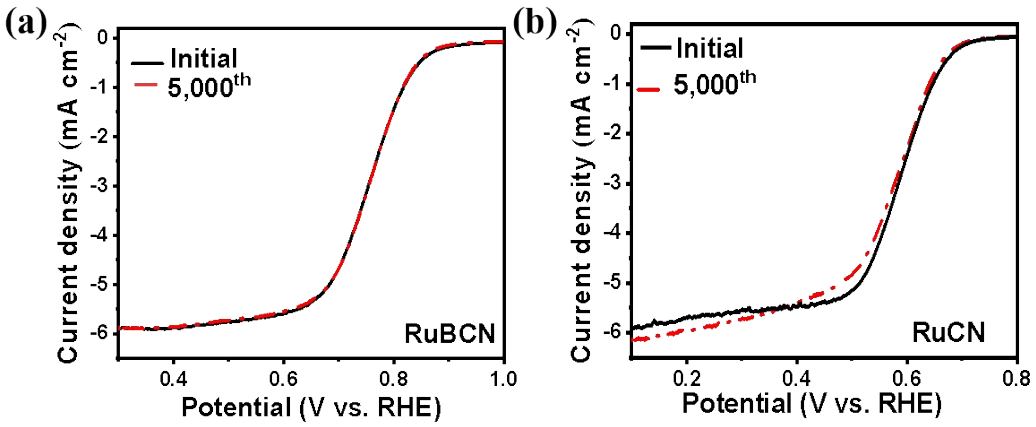

Fig S30. ORR stability test of RuBCN and RuCN in 0.1 M KOH electrolyte.

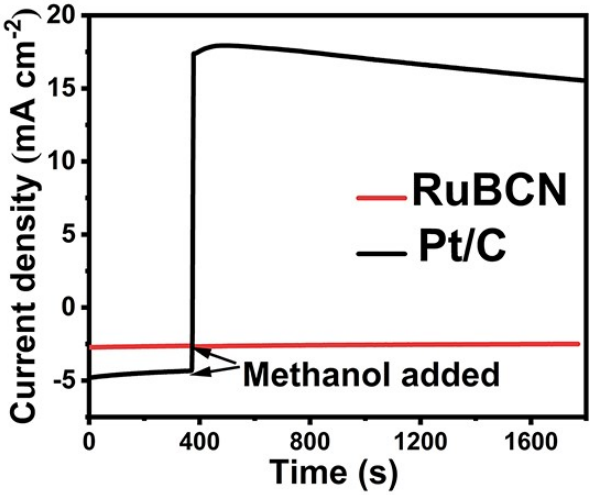

Fig S31. Chronoamperometric curves in 0.1 M KOH with the addition of methanol.

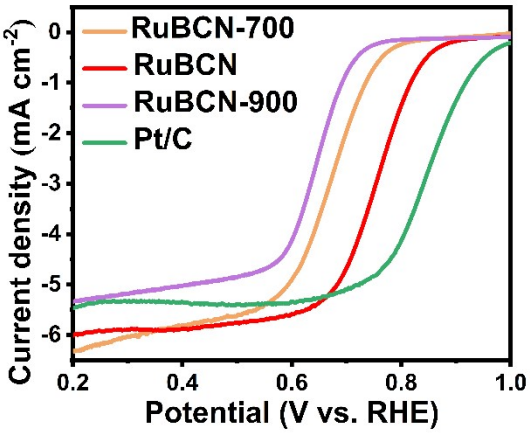

Fig S32. ORR polarization curve with scan rate of 5 mVs^{-1} at 1600 rpm of RuBCN-700, RuBCN and RuBCN-900.

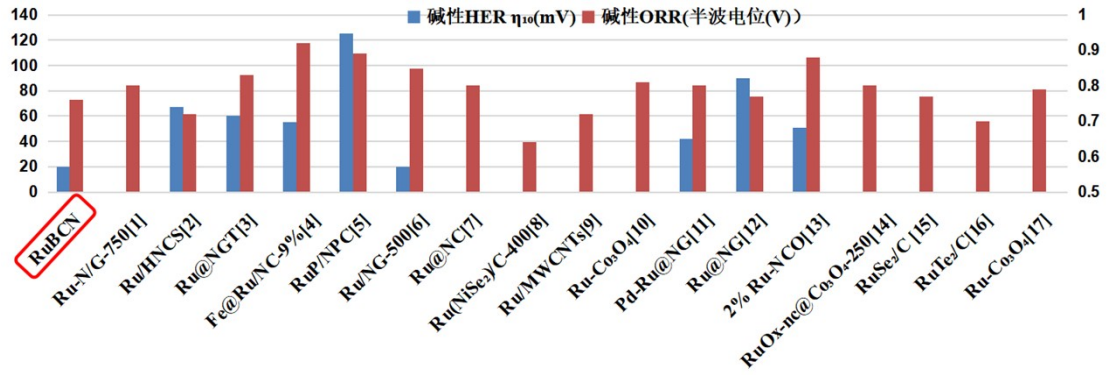

Fig S33. Performance comparison of HER (blue) and ORR (red) of relevant electrocatalyst, values in parentheses indicate reference numbers.

[1] Zhang C, Sha J, Fei H, et al. Single-Atomic Ruthenium Catalytic Sites on Nitrogen-Doped Graphene for Oxygen Reduction Reaction in Acidic Medium[J]. ACS Nano, 2017, 11(7): 6930-6941.

[2] Jiang A, Wang Z, Li Q, et al. An efficient ruthenium-based dual-electrocatalyst towards hydrogen evolution and oxygen reduction reactions[J]. Materials Today Physics, 2021, 16: 100300.

[3] Barman B K, Sarkar B, Ghosh P, et al. In Situ Decoration of Ultrafine Ru Nanocrystals on N-Doped Graphene Tube and Their Applications as Oxygen Reduction and Hydrogen Evolution Catalyst[J]. ACS Applied Energy Materials, 2019, 2(10): 7330-7339.

[4] Zong Z, Qian Z, Tang Z, et al. Hydrogen evolution and oxygen reduction reactions catalyzed by core-shelled Fe@Ru nanoparticles embedded in porous dodecahedron carbon[J]. Journal of Alloys and Compounds, 2019, 784: 447-455.

[5] Qin Q, Jang H, Chen L, et al. Low Loading of Rh_xP and RuP on N, P Codoped Carbon as Two Trifunctional Electrocatalysts for the Oxygen and Hydrogen Electrode Reactions[J]. Advanced Energy Materials, 2018, 8(29): 1801478.

[6] Liu S, Dai L, Qu Y, et al. Crystalline/amorphous hetero-phase Ru nanoclusters for efficient electrocatalytic oxygen reduction and hydrogen evolution[J]. Materials Chemistry Frontiers, 2021, 5(17): 6648-6658.

[7] Bisen O Y, Nanda K K. Uniform Distribution of Ruthenium Nanoparticles on Nitrogen-Doped Carbon Nanostructure for Oxygen Reduction Reaction[J]. ACS Applied Energy Materials, 2021, 4(11): 12191-12200.

[8] Liu J, Shen J, Gong Q, et al. Improving Nickel Diselenide Performance toward Oxygen Reduction Reaction with Ruthenium Incorporation and Heat Treatment[J]. Journal of The Electrochemical Society, 2022, 169(4): 044518.

[9] Liu C, Bai G, Jiao Z, et al. Particle size-control enables extraordinary activity of ruthenium nanoparticles/multiwalled carbon nanotube catalysts towards the oxygen reduction reaction[J]. Nanoscale, 2019, 11(29): 13968-13976.

[10] Hu D, Wang R, Du P, et al. Electrospinning Ru doped Co_3O_4 porous nanofibers as promising bifunctional catalysts for oxygen evolution and oxygen reduction reactions[J]. Ceram Int, 2022, 48(5): 6549-6555.
[11] Barman B K, Sarkar B, Nanda K K. Pd-coated Ru nanocrystals supported on N-doped graphene as HER and ORR electrocatalysts[J]. Chemical Communications, 2019, 55(92): 13928-13931.
[12] Zhang W, Xiao Y. Mechanism of Electrocatalytically Active Precious Metal (Ni, Pd, Pt, and Ru) Complexes in the Graphene Basal Plane for ORR Applications in Novel Fuel Cells[J]. Energy & Fuels, 2020, 34(2): 2425-2434.
[13] Zhang J, Lian J, Jiang Q, et al. Boosting the OER/ORR/HER activity of Ru-doped Ni/Co oxides heterostructure[J]. Chem Eng J, 2022, 439: 135634.
[14] Lu Q, Guo Y, Mao P, et al. Rich atomic interfaces between sub-1 nm RuO_x clusters and porous Co_3O_4 nanosheets boost oxygen electrocatalysis bifunctionality for advanced Zn-air batteries[J]. Energy Storage Materials, 2020, 32: 20-29.
[15] Gong Q, Hu P, Yang W, et al. Microwave-Assisted Preparation of the Cubic $RuSe_2$/C Catalyst for Fuel Cell Applications[J]. ACS Applied Energy Materials, 2022, 5(11): 13166-13175.
[16] Gong Q, Hu P, Zhang T, et al. Highly efficient $RuTe_2$/C electrocatalyst for oxygen reduction reaction in proton exchange membrane fuel cells[J]. Electrochim Acta, 2022, 436: 141334.
[17] Wang Y, Liu R, Xiao W, et al. Two-dimensional asymmetric structured Ru-Co based compounds as multifunctional electrocatalysts toward hydrogen/oxygen related applications[J]. Fuel, 2023, 334: 126635.